Late gas generation potential for different types of shale source rocks: Implications from pyrolysis experiments

Haifeng Gai, Hui Tian*, Xianming Xiao

State Key Laboratory of Organic Geochemistry, Guangzhou Institute of Geochemistry, Chinese Academy of Sciences, Guangzhou 510640, China

ABSTRACT

Gas generation from shale source rocks typically occurs via cracking of both kerogen and retained oils, such that it is difficult to predict and compare gas generation potentials of different shales because they are related not only to the kerogen type but also to the oil expulsion efficiency. In this study, five different shale kerogen samples were pyrolyzed in sealed gold tubes to investigate how kerogen type and oil expulsion efficiency affect their gas generation after oil-window maturity. The results illustrate that the maximum extractable organic matter (EOM) and gas generation potentials of different original shale kerogens (O-kerogen) in a closed system vary widely in the range of 229–790 mg/g TOC_{OK} and 308–594 mL/g TOC_{OK}, respectively. However, the gas yields of different residual shale kerogens (R-kerogen) with a starting equivalent vitrinite reflectance (EqVRo) value of approximately 1.22% are quite similar and vary between 131 and 145 mL/g TOC_{RK}. Pyrolysis experiments also reveal that the late gas generation potential (EqVRo > 1.22%) of shale is mainly controlled by the amount of retained EOMs rather than kerogen type. When the shale source rocks containing types I and II kerogens have the same amount of retained EOMs, their gas generation potentials are quite similar. Under most geological conditions, the late gas generation potentials of shale source rocks, normalized to the TOC of matured shale at 1.22% EqVRo (TOC_{Shale}), vary approximately in the range of 180–300 mL/g TOC_{Shale}. To reach a gas content of 3 m^3/ton shale for the present-day overmature shale gas exploration in the Lower Palaeozoic shales of South China, a conservative present-day TOC (TOC_{pd}) value of 2.0% is proposed as a screening parameter that can eliminate the risk of insufficient gas generation potential as much as possible.

1. Introduction

Gas exploration practice has shown that sufficient gas generation potential is one of the prerequisites for the formation of both conventional and unconventional gas pools (Galimov, 1988; Dai et al., 1997; Jarvie et al., 2007; Jarvie, 2012a). It has been recognized that, in addition to gas-prone source rocks containing type III kerogen or coals, organic-rich shale source rocks containing type I and II kerogens also have the ability to generate sufficient gas to form conventional gas reservoir and/or shale gas reservoir through cracking of retained oils in them (Curtis, 2002; Zhao et al., 2005; Hill et al., 2007; Jarvie et al., 2007; Jarvie, 2012a; Ma et al., 2007, 2008; Hao et al., 2008; Dai et al., 2014; Zou et al., 2014). Shale gas exploration activities in North America illustrate that the gas contents are largely positively related to the total organic carbon (TOC) content of shales (Curtis, 2002; Jarvie, 2012a), and the TOC content is usually used to screen the prospect area in the early stage of shale gas exploration because it is not only a measure of gas generation potential but also acts as a key control of

porosity of shales (Jarvie et al., 2007; Jarvie, 2012a; Curtis et al., 2012; Modica and Lapierre, 2012; Tian et al., 2013, 2015). At present, the cutoff value of TOC such as 1.0 or 2.0% is mainly estimated based on local exploration results (Curtis, 2002; Hill et al., 2007; Jarvie et al., 2007; Jarvie, 2012a). Therefore, a variable cutoff value of TOC would be expected when different shales and geological conditions are considered.

The term "late gas", sometimes also called "mature gas", usually refers to the hydrocarbon gas generated after the main stage of oil generation (Tissot and Welte, 1984; Lorant and Behar, 2002). Many factors may affect the late gas potential of shales, including kerogen type, oil expulsion efficiency, and thermal maturity levels (Behar et al., 1995, 1997; Pepper and Corvi, 1995; Erdmann and Horsfield, 2006; Jia et al., 2014; Gai et al., 2015). While the kerogen type and thermal maturity are relatively easy to determine, the oil expulsion efficiency of a shale bed is quite difficult to quantitatively evaluate because it may be affected by many geological factors, including the amount and physical property of oils generated, the migration pathway, the temperature and

pressure conditions of geological system, and so on (Leythaeuser et al., 1988; Sandvik et al., 1992; Lafargue et al., 1994; Pepper and Corvi, 1995; Ritter, 2003; Eseme et al., 2007; Uguna et al., 2012; Ziegs et al., 2017). In fact, oil expulsion efficiency measures only the proportion of oil that was expelled out of the source rocks (Cooles et al., 1986; Pepper and Corvi, 1995; Eseme et al., 2012); the amount of retained oils, which is jointly controlled by both oil generation potential and expulsion efficiency, directly determines the contribution of oil cracking gas to the late gas generation potential of shales (Jarvie et al., 2007; Jia et al., 2014; Gai et al., 2015). In addition, some retained EOM can be re-incorporated back into the residual kerogen and the neo-formation of more thermally stable organic matter may account for the late gas potential of overmature source rocks (Dieckmann et al., 2006; Erdmann and Horsfield, 2006; Mahlstedt et al., 2008; Mahlstedt and Horsfield, 2012). Mahlstedt and Horsfield (2012) conducted a systematic investigation on this topic and found that heterogeneous Type III or mixed II/III kerogens have a greater late gas potential than homogeneous Type I kerogen, indicating that aromatic and/or phenolic signatures are indicative of the possible presence of elevated late gas potential at high maturities.

Gas generation potentials of kerogens and crude oils are usually studied through laboratory pyrolysis experiments (Braun and Burnham, 1990; Behar et al., 1995, 1997; Pepper and Corvi, 1995; Berner and Faber, 1996; Dieckmann et al., 1998; Lorant and Behar, 2002; Erdmann and Horsfield, 2006; Hill et al., 2003, 2007; Jia et al., 2014; Xie et al., 2015). It has been recognized that oil cracking can produce a large amount of hydrocarbon gases during maturation process (Ungerer, 1988; Ungerer, 2003; Dieckmann et al., 1998; Hill et al., 2003; Tian et al., 2006, 2009, 2012) and the amount of retained oil is the main factor affecting the potential and evolution process of gas generation for shales, in particular for shales containing oil-prone kerogens (Hill et al., 2007; Jarvie et al., 2007; Jia et al., 2014; Gai et al., 2015). Previous studies either focused on a single type of shale source rock/kerogen (Gai et al., 2015; Xiong et al., 2016) or assumed specific oil expulsion conditions (Jia et al., 2014; Xie et al., 2015) to investigate the gas potential of shales, but the understanding and comparison of gas generation potential of different types of shale source rocks after oil expulsion still requires further investigation. In this study, five low-maturity shale samples were used to isolate original kerogen and prepare artificially matured kerogen samples, and the solvent-extractable organic matter (EOM) and gas generation potentials of the two series of kerogen samples were then investigated and compared via pyrolysis experiments, which may help evaluate the late gas generation potential of overmature shale source rocks required in shale gas exploration.

2. Samples and experiments

2.1. Geological background

Five shale core samples used in the present study were collected from two petroliferous basins: the Songliao Basin and the Bohai Bay Basin, in China (Table 1; Fig. 1a).

The Songliao Basin, which is one of the largest Meso-Cenozoic continental petroliferous basins in the world, is superposed onto a Palaeozoic basement in northeastern China and consists of six first-order tectonic units (Fig. 1b), including the Southwestern Uplift, Southeastern Uplift, Northeastern Uplift, Northern Plunge, Western Slope, and the Central Depression (Feng et al., 2010). As illustrated in Fig. 1c, the Upper Cretaceous sedimentary sequence comprises the Qinshankou (K_2qn), Yaojia (K_2y), Nenjiang (K_2n), Sifangtai (K_2s), and Mingshui (K_2m) formations, and the first members of K_2n and K_2qn formations (i.e., K_2n^1 and K_2qn^1) are the main source rocks in the Songliao Basin and were formed under the depositional environments of mediate-deep lakes (Jia et al., 2013; Cao et al., 2017).

The Bohai Bay Basin is a Cenozoic rift basin located in the eastern coast of China (Ye et al., 1985; Hsiao et al., 2004) and consists of seven

Table 1
Geochemical information of the shale samples obtained in this study.

Sample	Basin	Formation	Well	Depth (m)	TOC (%)	Ro (%)
A	Central Depression Songliao Basin	Cretaceous Nenjiang Fm	H151	1807.4	2.82	0.71
B	Jiyang Subbasin Bohai Bay Basin	Eocene Shahejie Fm	X47	2622.6	7.92	0.58
C	Jiyang Subbasin Bohai Bay Basin	Eocene Shahejie Fm	L10	3288.0	2.51	0.64
D	Jiyang Subbasin Bohai Bay Basin	Eocene Shahejie Fm	S743	3328.6	1.75	0.69
E	Jiyang Subbasin Bohai Bay Basin	Eocene Shahejie Fm	S743	3398.1	1.39	0.74

sub-basins, including the Linqing, Jizhong, Jiyang, Huanghua, Bozhong, Liaodong Bay, and Liaohe subbasins (Fig. 1d; Allen et al., 1997; Feng et al., 2016). Within the basin, the Paleogene sedimentary sequence comprises the Kongdian (E_2), Shahejie (Es), and Dongying (E_3) formations that were deposited primarily in lacustrine environments (Fig. 1e; Hu et al., 2001; Hao et al., 2011; Ma et al., 2017). The Shahejie Formation, which is the most important oil generating strata and reservoirs in the Bohai Bay Basin, is divided into four members and numbered as Es^1, Es^2, Es^3, and Es^4 from top to bottom (Fig. 1e; Guo et al., 2012; Ma et al., 2017).

2.2. Sample information

2.2.1. Shale core samples

One shale core sample was collected in the first member of the Nenjiang Formation (K_2n^1) with a present burial depth of 1807.4 m from well H151 in the Central Depression, the Songliao Basin (Fig. 1b), and was named 'Sample A'. This shale sample has a total organic carbon (TOC) content of 2.82% with a vitrinite reflectance (Ro) of 0.71% (Table 1).

Four other shale core samples were collected from the Shahejie Formation in the Jiyang Subbasin, the Bohai Bay Basin, and were named 'Sample B, C, D, and E', respectively. The Sample B is from the upper Es^4 Member of well X47 with a current burial depth of 2622.6 m, the Sample C is from the lower Es^3 Member of well L10 with a present burial depth of 3288.0 m, and the other two samples D and E are both from the upper Es^3 Member of well S743 and their respective burial depths are 3328.6 m and 3398.1 m (Table 1; Fig. 1d, e). As shown in Table 1, these four shale samples have respective TOC values of 7.92%, 2.51%, 1.75%, and 1.39%. The respective Ro values for Samples B, C, D, and E are 0.58%, 0.64%, 0.69%, and 0.74%. All the samples are in low maturity stage with respect to gas generation.

2.2.2. Sample preparation

The five shale samples were first crushed into powders (100 mesh) and then treated with hydrochloric and hydrofluoric acids (HCl and HF) to obtain original kerogen (O-kerogen) samples. Then these five O-kerogen samples were pyrolyzed in sealed quartz tubes at 380 °C for 24 h (Ro = 1.22%, measured from Sample E) and extracted with a methanol: acetone: benzene mixture (M: A: B = 2:5:5) for 72 h to recover the generated extractable organic matters (EOMs). The organic matter left in the pyrolyzed O-kerogen is termed residual kerogen (R-kerogen).

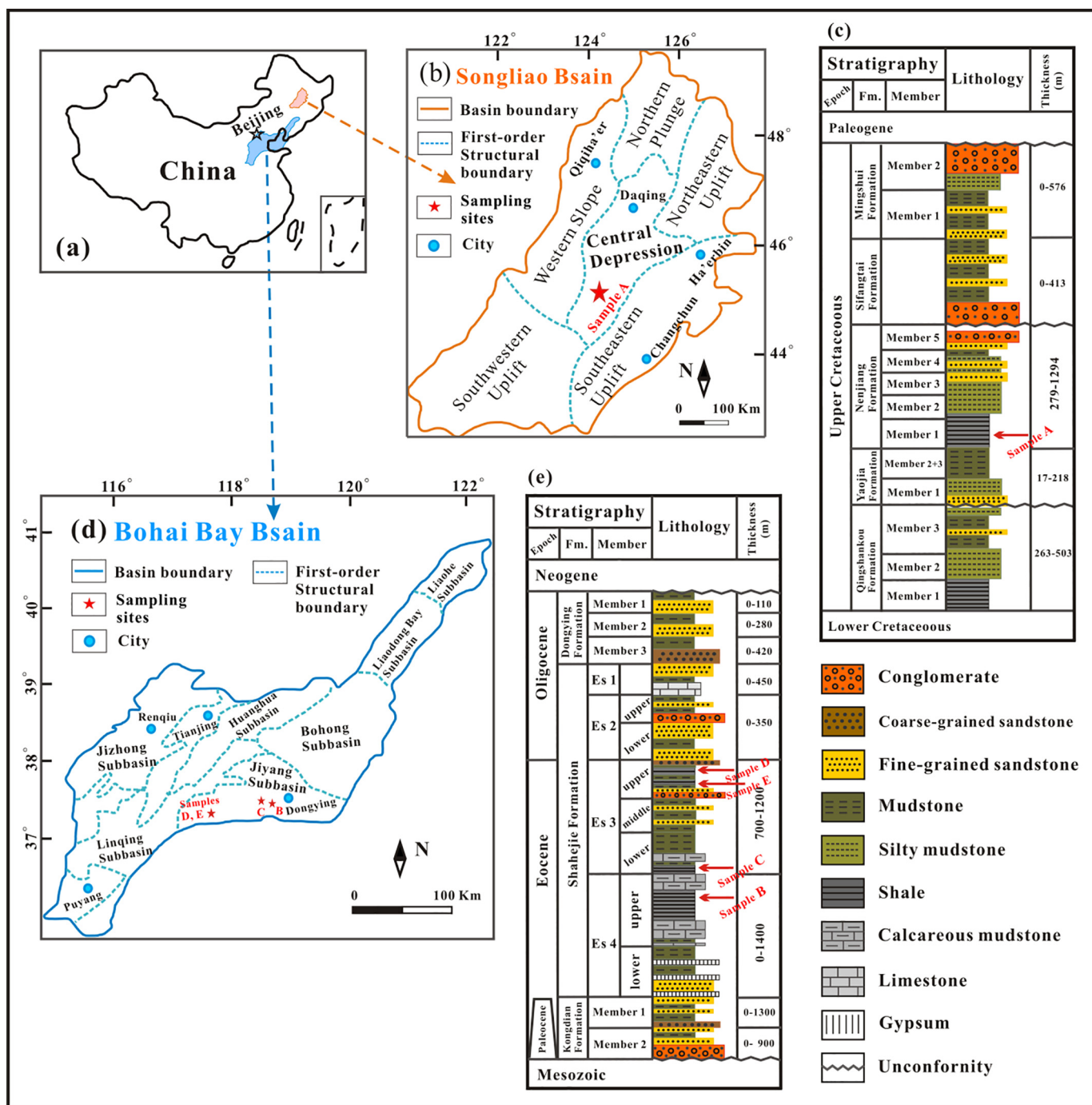The organic geochemical characteristics of the five O-kerogen

Fig. 1. Schematic maps showing the sampling locations. (a) Geographical location of the Bohai Bay Basin and the Songliao Basin. (b) First-order structural units of the Songliao Basin. (c) Stratigraphic columns of Upper Cretaceous sequence in the Songliao Basin. (d) Sub-basins of the Bohai Bay Basin. (e) Generalized Cenozoic stratigraphy of the Bohai Bay Basin. (b) and (c) are modified from Cao et al. (2017), and (d) and (e) are modified from Ma et al. (2017).

samples are listed in Table 2. Briefly, the Rock–Eval hydrogen index (HI) values for the five O-kerogen samples are in the range of 279–838 mg HC/g TOC$_{OK}$. The TOC$_{OK}$ here is used to indicate the TOC of O-kerogen samples. The original kerogen samples were plotted in the HI versus Tmax diagram adapted from Mukhopadhyay et al. (1995), illustrating that the organic matter in Sample A is typical of type I kerogen, Sample E contains type IIB kerogen which likely correspond to a mixture of terrestrial and aquatic organic matter, and the other three samples (B, C, and D) contain mainly type IIA kerogen (Fig. 2). Compared with the classification scheme of Peters and Cassa (1994), the Type IIA and Type IIB in this study are somehow equivalent to Type II

and Type II/III. After the O-kerogen samples were artificially matured to Ro = 1.22%, the HI values for the residual kerogen (R-kerogen) samples are in the range of 17–39 mg HC/g TOC$_{RK}$ (Table 2), indicating that their EOM potential is minor at further elevated thermal maturation. The TOC$_{RK}$ here is used to indicate the TOC of R-kerogen samples.

2.3. Pyrolysis experiment

Anhydrous pyrolysis experiments on the five O-kerogen samples and the five R-kerogen samples were performed using sealed gold tubes. Experimental details of this procedure have been described in literature

Table 2
Geochemical characteristics of the kerogen samples used in the pyrolysis experiments.

Sample	TOC_{OK} (%)	S_1 (mg/g)	S_2 (mg/g)	Tmax (°C)	HI (mg/g TOC_{OK})	Kerogen type
O-kerogen A	62.5	29.5	523.3	441	838	I
O-kerogen B	57.9	12.1	358.5	427	619	IIA
O-kerogen C	50.6	13.4	307.1	438	607	IIA
O-kerogen D	47.8	12.6	188.3	439	394	IIA
O-kerogen E	52.4	22.6	145.9	437	279	IIB

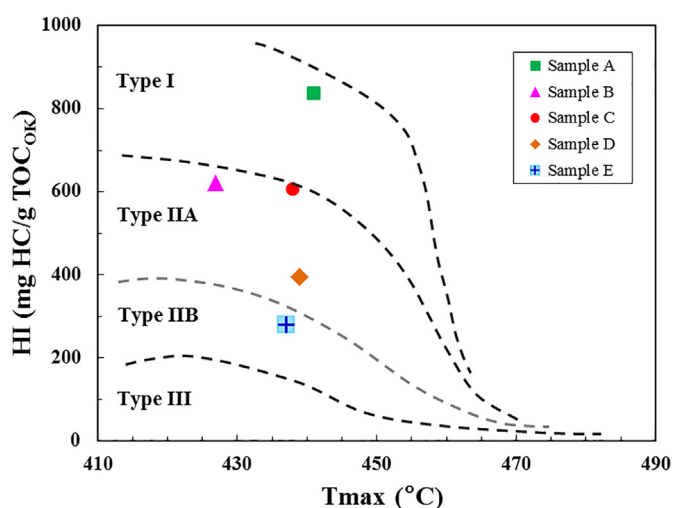| Sample	TOC_{RK} (%)	S_1 (mg/g)	S_2 (mg/g)	Tmax (°C)	HI (mg/g TOC_{RK})
R-kerogen A	40.2	0.61	14.67	474	36
R-kerogen B	46.7	0.84	18.29	463	39
R-kerogen C	40.5	0.68	9.61	470	24
R-kerogen D	43.3	0.37	7.23	472	17
R-kerogen E	50.6	0.39	9.73	468	19

Fig. 2. Plot of the Rock-Eval Hydrogen Index (HI) versus Tmax for the five O-kerogen samples. Classification of kerogen types adapted from Mukhopadhyay et al. (1995). The TOC_{OK} is used to indicate the TOC of O-kerogen samples.

(e.g., Xiao et al., 2005; Tian et al., 2012; Gai et al., 2015) and may be summarized as follows. Kerogen samples (50–200 mg) were filled into gold tubes that were pre-welded at one end (60 mm in length, 4 mm in inner diameter and 0.2 mm in wall thickness); each tube was flooded for 25 min with high purity argon to displace the residual air in the tube, then welded under the protection of argon gas and loaded into a stainless steel vessel.

Two types of pyrolysis experiments were performed in this study. The first one is mainly to investigate the oil (represented by EOM) generation potentials of the five O-kerogen samples, and the second is focused on the difference in gas generation between the O-kerogens and R-kerogens. Both types of pyrolysis experiments were conducted at a confining pressure of 50 MPa. The experimental temperature for the oil generation was first programmed from room temperature to 240 °C in 10 h, and then to 440 °C at a heating rates of 20 °C /h; for the gas generation experiment, the pyrolysis temperature was increased from room temperature to 240 °C in 10 h and subsequently to 600 °C at a heating rate of 2 °C/h. During experiments, the accuracy of temperature measurements was better than ± 0.5 °C and the accuracy of pressure measurements was ± 1 MPa. Once the target temperature was approached, the individual stainless vessel was withdrawn from the oven and rapidly cooled by quenching it in water.

2.4. Products analysis

For quantitative analysis of the EOM generated from O-kerogens,

the gold tube was immerged and opened in an 8-mL vial filled with MAB solvent as used for EOM extraction in Section 2.2. After two 30-min periods of ultrasonication, the vials with gold tubes were settled for 12 h. The solution in the vials was then filtered using a pre-extracted organic filter membrane (0.8 μm pore size). The organic solvent was allowed to evaporate at room temperature and atmospheric pressure until the weights of the filtrates were constant. Note that this procedure will lose the weight of volatile components such as gases and some light hydrocarbons, and such an underestimated yields of EOMs would lead to an overestimation of the gas potential of EOM-cracking gas. Nevertheless, these volatile components only account for a small part (approximately 3–7%) of the generated EOMs at the maturity of maximum cumulative EOM yield for Type I and II kerogens (Behar et al., 1997). As the present study is mainly focused on gas generation and the maximum EOM yield is only used to estimate the secondary cracking gas potential of retained EOMs, we did not perform a rigorous mass balance for all pyrolysates as required by compositional kinetic studies (Behar et al., 1997, 2006; Mahlstedt et al., 2008).

Carbon content of the EOM recovered at its peak yield was analyzed using a Vario EL III instrument (Elementar Analysensysteme GmbH). The experimental temperatures of the oxidation oven and reduction furnace were 1150 °C and 850 °C, respectively. Acetanilide (carbon element content of 71.09%) was used as a standard sample for calibration. The error ranges are less than ± 0.2%.

Gas composition of pyrolytic gases was analyzed using an Agilent 7890A gas chromatograph (GC) modified by Wasson ECE Instrumentation. The GC employed a Poraplot Q capillary column (30 m × 0.25 mm × 0.25 μm) with helium as carrier gas. The gas was injected into GC oven at a column temperature of 70 °C (held for 6 min), then the temperature was programmed at a rate of 15 °C/min to 180 °C and held for 4 min. The amounts of gaseous hydrocarbons (C_1–C_5) were quantified using an external standard method with a relative error < 0.5% (Pan et al., 2012). The gas volumes measured and reported in the present study are at SATP conditions (Standard Ambient Temperature and Pressure) with temperature of 25 °C and pressure of 101.325 kPa. At these conditions, one mole of an individual gas has a volume of approximately 24.5 L, and thus the gas yield measured in weight could be easily obtained with knowing the molecular weight of a specific gas.

2.5. Maturity calculation

In this study, the temperatures of the pyrolysis experiments were transformed into equivalent vitrinite reflectance (EqVRo) values for geological extrapolation. The experimental temperatures were first transformed into Easy%Ro values with the Easy%Ro model of Sweeney and Burnham (1990). The Easy%Ro model uses a chemical kinetic scheme to estimate a parameter known as the vitrinite conversion index (VCI), and the Easy%Ro value is then calculated from VCI using an empirical equation. However, Tang et al. (1996) found that the

Table 3
Yields of extractable organic matter (EOM) of the five O-kerogen samples at different pyrolysis temperatures.

Temperature (°C, 20 °C/h)	EqVRo (%)	EOM yield (mg/g TOC_OK)				
		O-kerogen A	O-kerogen B	O-kerogen C	O-kerogen D	O-kerogen E
320	0.62		44.3	58.6	54.1	
330	0.66	95.9	79.5	75.7	65.3	
350	0.74	188.5	149.6	156.8	117.1	97.2
370	0.81	441.7	338.0	324.2	263.8	157.3
390	0.90	790.1	561.7	538.7	382.6	229.4
410	1.02	789.3	532.1	575.3	352.6	217.7
440	1.26	653.9	474.2	496.3	277.5	184.2
M_O^a (mg/g TOC_OK)		790.1	561.7	575.3	382.6	229.4
C_O^b (%)		86.35	82.12	71.74	68.31	69.46

[a] M_O: the maximum yield of EOM that incudes already-generated hydrocarbons as measured by S_1 peak of Rock-Eval analysis.

[b] C_O: percentage of element carbon of generated EOM at its peak yield.

empirical relationship between VCI and Ro as used in the Easy%Ro model overestimates the vitrinite reflectance at higher maturity levels but underestimates the vitrinite reflectance at lower maturity levels. Therefore, they fitted a new regression equation between the VCI values calculated by the kinetic parameters as used in Easy%Ro model and the measured Ro values of coal samples. Using this newly fitted equation of Tang et al. (1996), the Easy%Ro values were further converted into equivalent vitrinite reflectance (EqVRo) values. The EqVRo values for our pyrolysis temperatures are in the range of 1.25–3.58%, covering the main thermal maturity range of gas generation under geological conditions.

3. Results and discussion

3.1. Extractable organic matter yields from O-kerogens

The yields of extractable organic matter (EOM) generated from the five O-kerogen samples are listed in Table 3. Briefly, the EOM yields increase steadily until their maxima are approached at 0.9–1.02% EqVRo, and then they begin to decrease rapidly due to secondary cracking. As shown in Table 3, the maximum yields of EOM generated from the five original kerogens vary significantly, ranging from the highest value of 790.1 mg/g TOC_OK for the type I O-kerogen (Sample A), through 382.6–575.3 mg/g TOC_OK for the three type IIA O-kerogens (Samples B, C, and D), to the smallest value of 229.4 mg/g TOC_OK for the type IIB O-kerogen (Sample E). Note that the maximum yields of EOMs for our samples are all close to their HI values. One reason for this phenomenon is that the EOMs in our study include both S_1 and S_2 peaks whereas HI values are obtained only from S_2 peaks (Lafargue et al., 2006). Furthermore, a variation in elemental carbon content is also observed among the EOMs recovered from different types of kerogens at their peak yields (Table 3). Generally, the carbon contents of the EOM from type I and IIA O-kerogens are higher than those of the type IIB O-kerogen. This variation reflects the distinct elemental composition of O-kerogens and further indicates that type IIB kerogen typically has higher contents of N, S, and O than type I and IIA kerogens (Tissot and Welte, 1984), leading to more non-hydrocarbon compounds in the pyrolysis products.

3.2. Gaseous hydrocarbon yields of O-kerogens

The amounts of gaseous hydrocarbons generated from the five O-kerogen samples are listed in Table 4 and plotted in Fig. 3. The methane yields (C_1) are quite similar for all samples at the early pyrolysis stage (EqVRo ≤ 1.93%), but become distinct when EqVRo values are greater than 1.93% (Fig. 3a). For example, the respective methane yields at EqVRo = 1.93% for the type I O-kerogen (Sample A), type IIA O-kerogen (Sample D), and type IIB O-kerogen (Sample E) are 145.2, 148.1, and 131.3 mL/g TOC_OK, with a variation of only 16.8 mL/g

TOC_OK. At EqVRo = 3.58%, their respective methane yields are 584.3, 388.0, and 306.9 mL/g TOC_OK, with a variation of up to 277.4 mL/g TOC_OK (Table 4). By contrast, the yields of C_2 through C_5 hydrocarbons ($C_{2–5}$) for various types of O-kerogens track differently throughout the entire pyrolysis process (Fig. 3b). The maximum difference occurs at EqVRo = 1.93%, and corresponds to the $C_{2–5}$ peak yields. For the type I O-kerogen (Sample A), the $C_{2–5}$ peak yield is as high as 180.8 mL/g TOC_OK, whereas it is only 87.4 mL/g TOC_OK for the type IIA O-kerogen (Sample D), and even as low as 51.0 mL/g TOC_OK for the type IIB O-kerogen (Sample E) (Table 4; Fig. 3b). Beyond 1.93% EqVRo, the $C_{2–5}$ hydrocarbon yields begin to decrease, which is attributed to their cracking to methane and pyrobitumen (Hill et al., 2003). Nevertheless, differences in $C_{2–5}$ yields among the three types of O-kerogens are still evident. For example, the yield of $C_{2–5}$ gases from the type IIB O-kerogen sample becomes negligible (< 1 mL/g TOC_OK) at 3.0% EqVRo, whereas the type I O-kerogen still produces a small amount of ethane (approximately 5.8 mL/g TOC_OK) at 3.58% EqVRo (Fig. 3b).

As illustrated in Fig. 3c, the yields of total hydrocarbon gases ($C_{1–5}$) for O-kerogens constantly increase with increasing maturity and show the order of type I > type IIA > type IIB. Like the gas yields, the dryness index values (volume ratio of $C_1/C_{1–5}$, %) for the generated hydrocarbon gases also show significant variations among the different O-kerogens types (Fig. 3d). In general, the dryness indices for oil-prone kerogens are lower than those for gas-prone kerogens at similar thermal maturity (i.e., type I < type IIA < type IIB) because type I O-kerogen can generate more wet gases ($C_{2–5}$) than type IIA and IIB O-kerogens (Fig. 3b). During the early pyrolysis stage (EqVRo ≤ 1.93%), the dryness indices for samples A, B, and C with a higher oil (EOM in this study) potential decrease gradually, whereas they display a monotonic increase for samples D and E, which have a lower EOM potential. Once the thermal maturity is greater than 1.93% EqVRo, the wet gases begin to crack into methane and pyrobitumen (Fig. 3b) and the dryness indices for all samples increase rapidly in a similar way (Fig. 3d).

3.3. Gaseous hydrocarbon yields of R-kerogens

The yields and chemical compositions of hydrocarbon gases generated from the five R-kerogen samples are listed in Table 5 and compared in Fig. 4. It is evident that the methane yields for different R-kerogen samples are quite similar throughout the pyrolysis stage. With increasing maturity levels, the methane yields increase steadily up to 3.02% EqVRo and then level out (Fig. 4a). When the thermal maturity evolves to 3.58% EqVRo, the maximum methane yields for the five R-kerogen samples are in the ranges of 130.2–144.5 mL/g TOC_RK (Table 5), approximately reduced by 55–75% compared to those of the O-kerogens (Table 4). Furthermore, the difference in methane yields for the five R-kerogens at 3.58% EqVRo is only 14.3 mL/g TOC_RK, which is considerably lower than that for the five O-kerogens (i.e., 277.4 mL/g TOC_OK) (Table 4). The $C_{2–5}$ gases generated from the R-kerogens are

Table 4
Gaseous hydrocarbon yields for the five O-kerogen samples at different pyrolysis temperatures.

Sample	Temperature (°C, 2 °C/h)	EqVRo (%)	Gas yield* (mL/g TOC_{OK})							
			C_1	C_2	C_3	C_4	C_5	C_{2-5}	C_{1-5}	C_1/C_{1-5} (%)
A	400	1.25	34.18	14.23	9.96	5.53	1.46	31.17	65.35	52.30
	420	1.44	55.01	22.79	17.91	9.93	2.72	53.35	108.36	50.77
	440	1.68	100.21	50.12	44.81	24.78	6.01	125.73	225.94	44.35
	460	1.93	145.17	75.10	62.97	33.12	9.60	180.79	325.96	44.54
	480	2.20	233.55	101.82	62.93	15.15	0.77	180.67	414.23	56.38
	500	2.48	315.93	108.99	39.42	5.02	0.27	153.70	469.63	67.27
	520	2.72	397.07	107.71	18.99	1.51	0.12	128.32	525.39	75.58
	540	3.02	478.16	82.57	2.03	0.19		84.80	562.95	84.94
	560	3.24	533.52	50.41	0.74	0.11		51.27	584.79	91.23
	580	3.43	573.34	19.84	0.31	0.06		20.22	593.57	96.59
	600	3.58	584.26	5.76	0.13			5.89	590.15	99.00
B	400	1.25	42.53	20.07	10.50	3.87	0.96	35.40	77.93	54.57
	420	1.44	61.48	28.32	17.44	8.63	2.87	57.26	118.74	51.78
	440	1.68	103.63	48.38	32.89	17.19	5.66	104.13	207.76	49.88
	460	1.93	154.41	62.51	39.97	17.08	3.32	122.87	277.29	55.69
	480	2.20	228.16	72.63	34.71	7.28	0.26	114.89	343.04	66.51
	500	2.48	295.77	73.19	20.08	1.94	0.06	95.27	391.04	75.64
	520	2.72	362.54	61.08	6.61	0.34		68.03	430.57	84.20
	540	3.02	435.71	29.00	0.47	0.05		29.52	465.23	93.65
	560	3.24	474.77	8.09	0.13			8.22	482.99	98.30
	580	3.43	479.81	1.86	0.06			1.92	481.74	99.60
	600	3.58	480.47	1.45	0.08			1.53	482.00	99.68
C	400	1.25	35.58	18.31	10.06	4.48	1.31	34.15	69.73	51.03
	420	1.44	52.27	24.26	14.05	6.75	2.23	47.29	99.56	52.50
	440	1.68	97.11	42.76	28.94	15.22	5.14	92.07	189.18	51.33
	460	1.93	146.98	61.75	41.41	18.57	4.27	126.01	272.99	53.84
	480	2.20	217.61	73.03	39.01	10.96	0.75	123.75	341.36	63.75
	500	2.48	304.14	65.18	18.68	2.00	0.09	85.96	390.10	77.96
	520	2.72	387.54	41.89	4.63	0.29		46.80	434.34	89.23
	540	3.02	455.97	10.61	0.33	0.06		11.00	466.97	97.64
	560	3.24	495.96	2.09	0.12	0.05		2.26	498.22	99.55
	580	3.43	505.29	1.50	0.06			1.56	506.85	99.69
	600	3.58	505.63	1.42				1.42	507.05	99.72
D	400	1.25	37.21	16.08	7.94	3.34	1.02	28.38	65.60	56.72
	420	1.44	55.51	21.79	11.25	5.04	1.68	39.75	95.25	58.28
	440	1.68	100.61	35.56	19.95	8.43	2.09	66.02	166.63	60.38
	460	1.93	148.14	51.05	25.01	9.55	1.81	87.42	235.56	62.89
	480	2.20	215.72	52.88	18.32	4.01	0.20	75.41	291.13	74.10
	500	2.48	280.07	25.63	8.19	1.58	0.05	35.45	315.52	88.76
	520	2.72	341.00	6.89	0.45	0.15		7.49	348.49	97.85
	540	3.02	370.53	1.08	0.11	0.06		1.25	371.78	99.66
	560	3.24	388.00	0.97	0.07	0.05		1.10	389.10	99.72
	580	3.43	389.00	0.88				0.88	389.88	99.77
	600	3.58	388.00	0.79				0.79	388.79	99.80
E	400	1.25	28.09	12.36	5.32	1.97	0.54	20.19	48.27	58.19
	420	1.44	44.31	16.71	7.44	2.86	0.82	27.83	72.14	61.42
	440	1.68	88.37	28.02	13.39	5.36	1.50	48.28	136.65	64.67
	460	1.93	131.33	33.30	13.06	4.07	0.60	51.03	182.37	72.01
	480	2.20	196.90	28.80	5.48	0.90		35.19	232.09	84.84
	500	2.48	250.34	8.87	0.40	0.06		9.34	259.68	96.40
	520	2.72	285.92	1.33	0.06			1.39	287.31	99.52
	540	3.02	298.66	0.83				0.83	299.49	99.72
	560	3.24	304.05	0.72				0.72	304.77	99.76
	580	3.43	306.00	0.70				0.70	306.70	99.77
	600	3.58	306.92	0.66				0.66	307.58	99.79

*The weight yield (mg/g TOC_{OK}) can be obtained by dividing the volume yield (mL/g TOC_{OK}) by 24.5 and then being multiplied by the mole mass of individual gas.

dominated by ethane (Table 5) and their maximum yields are as low as 1.5–7.8 mL/g TOC_{RK} (Fig. 4b), so the amounts of total gaseous hydrocarbons are quite similar to those of methane (Table 5).

Although some variations in the dryness indices of the hydrocarbon gases for the five R-kerogens are observed during the early pyrolysis stage (EqVRo ≤ 1.93%), they are largely similar at higher thermal maturity levels (Fig. 4c). Compared to the results of O-kerogens (Fig. 3d), gases from R-kerogens are much drier. For example, the values of dryness index for the five R-kerogens are greater than 95% at 1.93% EqVRo and even greater than 99% at EqVRo > 2.5% (Fig. 4c). These results illustrate that whatever the kerogen type is, the gases

derived from kerogen itself from end of oil window (1.22% EqVRo) and throughout the gas window maturity are always dominated by methane, and the high abundance of C_{2-5} wet gases observed for O-kerogens is mainly related to the cracking of oils (or EOMs) retained in them.

3.4. Influence of retained EOM on gas generation potential

As mentioned above, hydrocarbon gases generated from O-kerogens include both kerogen- and EOM-cracking gases, whereas for R-kerogens, they are dominated by kerogen-cracking gases starting from an
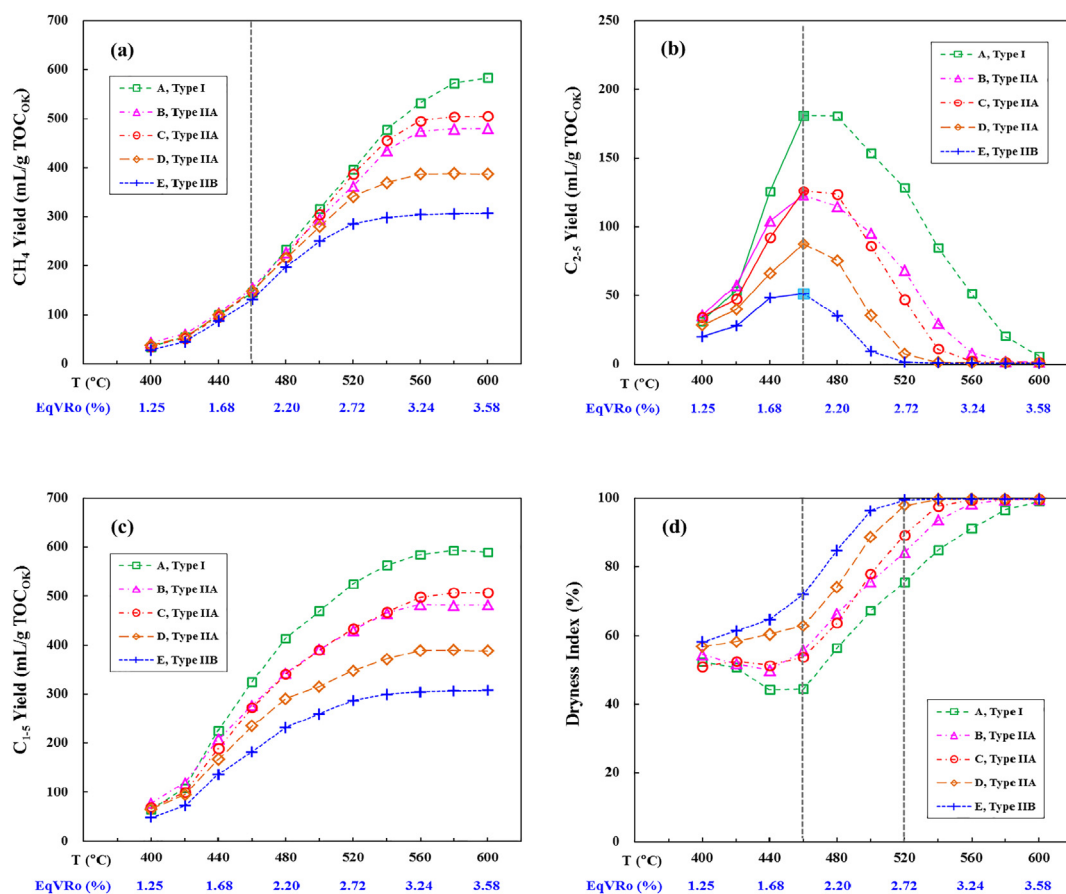
Fig. 3. Yields of C_1 through C_5 hydrocarbons and dryness indices (volume ratio of C_1/C_{1-5}, %) for the five O-kerogens samples during thermal evolution. The gas yields are normalized to the total organic carbon contents of O-kerogens (TOC_{OK}). Significant differences in yields and chemical compositions of pyrolytic gases after pyrolysis up to different maturity levels exist among different samples.

EqVRo value of approximately 1.22%. Therefore, the plots of gas yields versus EOM generation potentials for O-kerogens can be used to investigate the contribution of cracking of EOM in a closed system to the total gas yield. As shown in Fig. 5a, the C_{1-5} gas yields are evidently controlled by both the EOM generation potential (i.e., kerogen type) and the thermal maturity. At the early stage of gas generation (EqVRo ≤ 1.44%), there is only a weak correlation between C_{1-5} gas yield and EOM generation potential because conversion of EOM to gas has not extensively occurred. With increasing thermal maturity, more and more EOM-cracking gases are generated, which are manifested by the increase in the slopes of the linear regression for the C_{1-5} yield and EOM generation potential. In fact, the linear relationship in Fig. 5a reveals that the yields of gas derived from the cracking of per unit mass EOM (mg) retained in the five O-kerogen samples are quite similar and the slope values represent the yields of EOM-cracking gas at given thermal maturity level (e.g. 0.128 mL/mg EOM, i.e. 128 mL/g EOM at EqVRo = 1.68%). At Ro = 3.58%, the cumulative yield of gases from the cracking of EOM is approximately 481 mL/g EOM (0.481 mL/mg EOM in Fig. 5a). This value is lower than the gas generation potentials of crude oils that are reported to be in the range of 550–600 mL/g oil at the same thermal maturity level (Tian et al., 2006, 2009, 2012; Guo et al., 2009; Pan et al., 2010) but is largely consistent with the gas generation potential of artificially generated and extracted EOMs (Gai et al., 2015; Fig. 5b). The lower gas yield for artificially generated oils or EOMs may be attributed to their less enrichment in hydrogen-rich fractions such as saturates (Behar et al., 1997) that have a much higher gas potential than other fractions such as aromatics, resins and asphaltenes (Tian et al., 2012) and pyrobitumen formation (Hill et al., 2003). Note that the retained oils in shale source rocks may be more

similar to the artificially generated and extracted oils (EOMs) than the reservoired crude oils with respect to their relative components of saturates, aromatics, resins and asphaltenes (SARA) when migration fractionation in geological conditions is taken into account (Leythaeuser et al., 1984, 1988; Stainforth and Reinders, 1990; Sandvik et al., 1992; Eseme et al., 2007).

Similar to the yields of total gaseous hydrocarbons, the yield of individual gaseous component is also controlled by the amount of EOM. Fig. 6a shows a linearly positive correlation between the maximum yield of individual gas component and the amount of EOM for the O-kerogens. The slopes of linearly regressed lines gradually increase with decreasing molecular weight of hydrocarbon gas, ranging from 14.9 for C_5 to 503.4 for methane. This trend indicates that the EOM have a more pronounced influence on gases of lower molecular weights, which can be explained by the cracking of gases of higher molecular weight to methane and other gases of lower molecular weights (Hill et al., 2003). Therefore, the amounts of EOM retained in O-kerogens will significantly change both the yields and chemical compositions of hydrocarbon gases generated in a closed system. For the R-kerogen samples, their maximum methane yields are, however, not associated with their original EOM potentials (Fig. 6b), indicating that the gas potential of different types of mature kerogen tends to be similar after 1.22% EqVRo. Although the ethane generated from R-kerogens are extremely limited, its yield is still positively related to the original EOM potentials of R-kerogens (Fig. 6b). This suggests that the original characteristics of R-kerogens can still be revealed by valuable information such as ethane yield or gas dryness, though they evolve to be similar with respect to gas generation at overmature stages (i.e., EqVRo > 2.0%) when their generated EOM are completely expelled and/or thermally decomposed.

Table 5
Gaseous hydrocarbon yields for the five R-kerogen samples at different pyrolysis temperatures.

Sample	Temperature (°C, 2 °C/h)	EqVRo (%)	Gas yield* (mL/g TOC$_{RK}$)						
			C$_1$	C$_2$	C$_3$	C$_4$	C$_{2-5}$	C$_{1-5}$	C$_1$/C$_{1-5}$ (%)
A	400	1.25	17.40	5.14	0.69	0.04	5.87	23.27	74.77
	420	1.44	31.95	6.97	0.80	0.04	7.82	39.77	80.34
	440	1.68	57.27	5.55	0.19		5.74	63.01	90.89
	460	1.93	80.47	3.44			3.44	83.91	95.90
	480	2.20	100.23	1.34			1.34	101.57	98.68
	500	2.48	115.53	0.69			0.69	116.22	99.41
	520	2.72	128.15	0.41			0.41	128.56	99.68
	540	3.02	133.77	0.34			0.34	134.11	99.75
	560	3.24	137.41	0.26			0.26	137.67	99.81
	580	3.43	138.01	0.22			0.22	138.23	99.84
	600	3.58	138.97	0.19			0.19	139.16	99.86
B	400	1.25	14.36	2.46	0.16		2.63	16.98	84.57
	420	1.44	28.87	3.56	0.17		3.72	32.59	88.59
	440	1.68	53.89	2.99	0.07		3.06	56.95	94.63
	460	1.93	75.93	2.25	0.02		2.27	78.20	97.10
	480	2.20	95.92	1.19	0.04		1.23	97.15	98.73
	500	2.48	110.06	0.41			0.41	110.47	99.63
	520	2.72	118.76	0.45			0.45	119.21	99.62
	540	3.02	125.06	0.26			0.26	125.32	99.79
	560	3.24	128.23	0.24			0.24	128.47	99.81
	580	3.43	130.02	0.20			0.20	130.22	99.85
	600	3.58	130.16	0.18			0.18	130.34	99.86
C	400	1.25	6.39	0.98			0.98	7.37	86.70
	420	1.44	15.78	2.11			2.11	17.89	88.21
	440	1.68	41.04	2.71			2.71	43.75	93.81
	460	1.93	63.89	1.71			1.71	65.60	97.39
	480	2.20	86.20	1.07			1.07	87.28	98.76
	500	2.48	106.34	0.60			0.60	106.94	99.44
	520	2.72	122.38	0.44			0.44	122.82	99.64
	540	3.02	132.47	0.32			0.32	132.79	99.76
	560	3.24	136.46	0.26			0.26	136.72	99.81
	580	3.43	138.48	0.23			0.23	138.71	99.83
	600	3.58	138.87	0.18			0.18	139.05	99.87
D	400	1.25	6.21	0.90			0.90	7.11	87.34
	420	1.44	16.26	2.04			2.04	18.30	88.85
	440	1.68	48.00	3.19			3.19	51.19	93.77
	460	1.93	72.98	2.18			2.18	75.15	97.11
	480	2.20	94.24	1.10			1.10	95.34	98.85
	500	2.48	110.42	0.46			0.46	110.88	99.59
	520	2.72	120.48	0.28			0.28	120.76	99.77
	540	3.02	128.36	0.20			0.20	128.56	99.84
	560	3.24	132.60	0.20			0.20	132.80	99.85
	580	3.43	133.94	0.20			0.20	134.14	99.85
	600	3.58	134.26	0.19			0.19	134.45	99.86
E	400	1.25	6.12	0.55			0.55	6.67	91.75
	420	1.44	14.64	1.13			1.13	15.77	92.83
	440	1.68	42.22	1.45			1.45	43.68	96.66
	460	1.93	66.37	0.76			0.76	67.13	98.87
	480	2.20	88.68	0.35			0.35	89.03	99.61
	500	2.48	114.51	0.23			0.23	114.74	99.80
	520	2.72	132.38	0.20			0.20	132.58	99.85
	540	3.02	141.19	0.18			0.18	141.37	99.87
	560	3.24	142.10	0.18			0.18	142.28	99.87
	580	3.43	143.80	0.18			0.18	143.98	99.87
	600	3.58	144.48	0.17			0.17	144.65	99.88

* The weight yield (mg/g TOC$_{RK}$) can be obtained by dividing the volume yield (mL/g TOC$_{RK}$) by 24.5 and then being multiplied by the mole mass of individual gas.

3.5. Late gas generation potential for shale source rock

3.5.1. Calculation methods of the late gas generation potential

The pyrolysis experiments in this study represent the gas generation potentials in two extreme geological conditions where the generated EOM are either completely retained or expelled from the shale source rocks. However, only part of the generated EOMs would be retained in the shales after oil expulsion under most geological conditions (Cooles et al., 1986; Ozkaya and Akbar, 1991; Pepper and Corvi, 1995; Ritter, 2003; Eseme et al., 2007; Wei et al., 2012; Ziegs et al., 2017); therefore, the gas generation potential of a shale actually falls between the gas yields of O-kerogen and R-kerogen investigated here and is directly controlled by the amount of retained EOMs. Previous studies show that some of the generated oils (EOMs in this study) would be adsorbed onto kerogens and cannot be expelled out of the shale source rocks (Sandvik et al., 1992; Ritter, 2003; Jarvie, 2012b). The amount of adsorbed oils (or EOMs) for shales containing type I and type II kerogens are approximately 80 mg/g TOC$_{Shale}$ (Jarvie, 2012b; Li et al., 2016; Cao et al., 2017) and the term TOC$_{Shale}$ refers to the total organic carbon of both residual kerogen and retained EOMs in a matured shale that has been depleted of oil generation potential. In other words, no liquid organic matter would be further expelled out of the shale source rocks when the
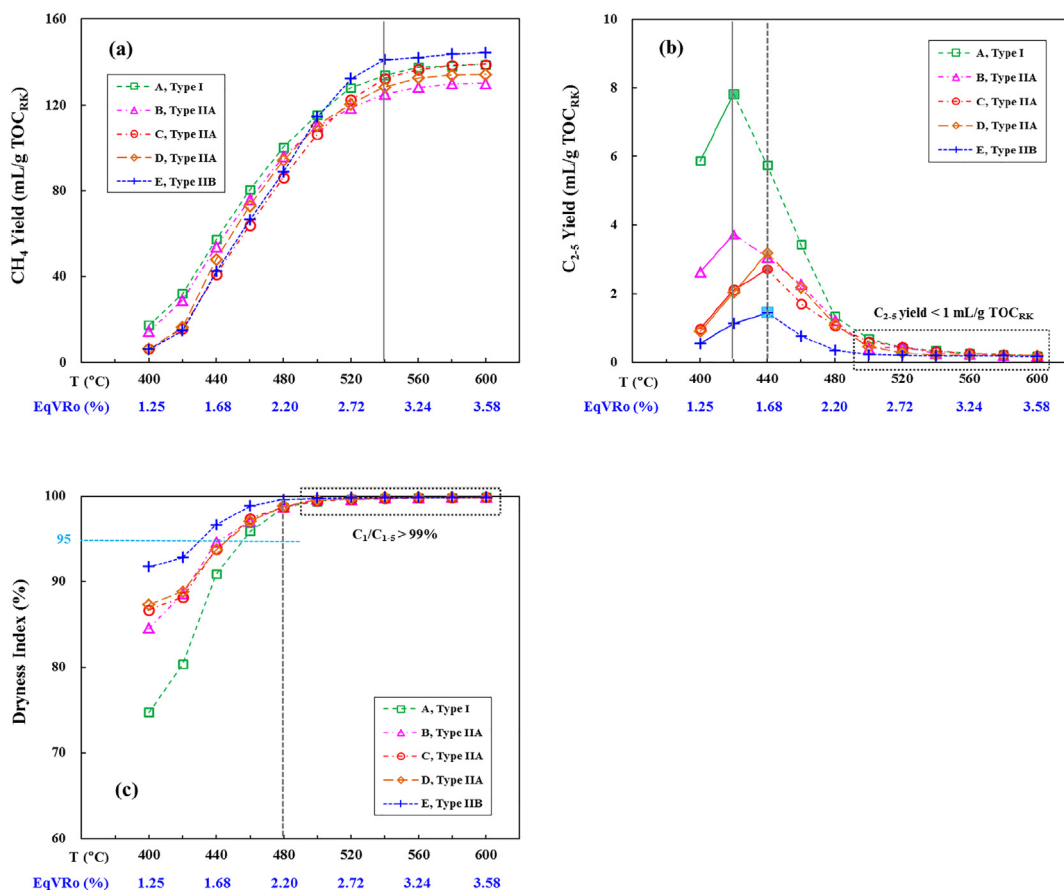
Fig. 4. Yields of C_1 through C_5 hydrocarbons and dryness indices for the five R-kerogens samples after pyrolysis up to different maturity levels. The gas yields are normalized to the total organic carbon contents of R-kerogens (TOC_{RK}). The trends for gas yields and chemical compositions of different samples are quite similar.

amount of retained liquid organic matter (or oils) in the source rocks is reduced to 80 mg/g TOC_{Shale} during the process of oil expulsion. According to the EOM generation potential of different types of O-kerogens investigated in this study (Table 3), the amount of retained EOMs in the shales can be calculated for different oil expulsion efficiencies (Fig. 7a). When the amount of retained EOM in shales containing different types of kerogens decreases to 80 mg/g TOC_{Shale}, their oil expulsion efficiencies are approximately 70% (Sample E, type IIB kerogen), 84% (Sample D, type IIA kerogen), and 95% (Sample A, type I kerogen), respectively (Fig. 7a).

The gas generated from a shale source rock after oil expulsion can be considered as the sum of the gas from the cracking of residual kerogens and retained EOM. In present study, the gas yields of residual kerogens are measured directly whereas those of retained EOM are calculated by comparing the gas generation potential of O-kerogen and R-kerogen samples (Fig. 5). Based on these results, the late gas generation potential of different types of source rocks can be further calculated at any given thermal maturity. Taking the 3.5% EqVRo as an example, the main procedures are illustrated as below.

(a) The gas yields of R-kerogens and retained EOM are denoted by Y_K (see details in Table 5) and Y_O, respectively.
(b) The amounts of retained EOM (M_{RO}) that are normalized to the TOC of O-kerogen (TOC_{OK}) are calculated using Eq. (1):

$$M_{RO} = \frac{M_O}{1000} \times (100\% - EE\%) \tag{1}$$

where M_O is the maximum yields (mg/g TOC_{OK}) of generated EOM (see details in Table 3), EE% represents the oil (or EOM in this study) expulsion efficiency, and M_{RO} is in unit of g/g TOC_{OK}.

(c) The TOC of R-kerogen (TOC_{RK}) is related to the TOC_{OK} through Eq. (2):

$$TOC_{RK} = TOC_{OK} \times \left(1 - \frac{M_O}{1000} \times C_O\%\right) \tag{2}$$

where C_O is the percentage of element carbon of generated EOM (see details in Table 3).

(d) The amounts of retained EOM (M_R) that are normalized to the TOC_{RK} are calculated by combining Eqs. (1) and (2),

$$M_R = \frac{1}{1 - \frac{M_O}{1000} \times C_O\%} \times \frac{M_O}{1000} \times (100\% - EE\%) \tag{3}$$

(e) The gas yield of retained EOM (at 3.5% EqVRo) can be calculated according to Eq. (4):

$$Y_O = 481 \times M_R \tag{4}$$

In Eqs. (4), the values of 481 represent the EOM-cracking gas yield at 3.5% EqVRo is 481 mL/g retained EOM (see details in Fig. 5 and Section 3.4).

(f) The gas generation potential for the shale is calculated using Eq. (5) and was normalized to mL/g TOC_{Shale}, and the TOC_{Shale} indicates the total organic carbon content of the matured shale that contains both residual kerogen and retained EOMs Eq. (6):

$$Y = \frac{Y_K + Y_O}{1 + M_R \times C_O\%} \tag{5}$$

$$TOC_{Shale} = TOC_{RK} \times (1 + M_R \times C_O\%) \tag{6}$$
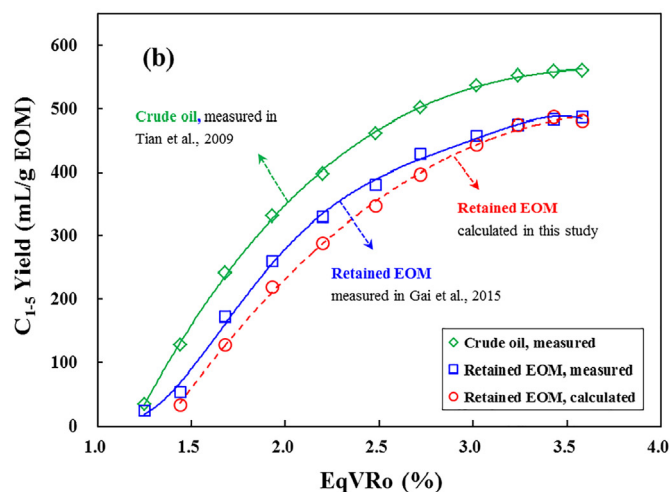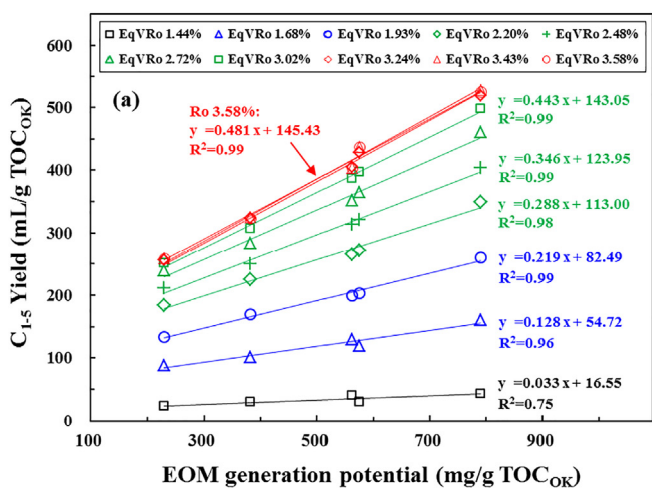
Fig. 5. (a) Relationship between the gas yields and EOM generation potentials for O-kerogens in a closed system, and (b) a comparison of the gas yields of retained EOM calculated from the slope values of the linear equations in (a) with the measured gas yields of crude oil and retained EOM from Tian et al. (2009) and Gai et al. (2015), respectively. Gas yields of O-kerogens are corrected for the cumulative associated gas generated in the oil window (i.e., before 1.25% EqVRo).

(g) The contribution of the retained EOM to the late gas yields of shales (*f*) can be calculated according to Eq. (7):

$$f = \frac{Y_O}{Y_K + Y_O} \times 100\% \tag{7}$$

According to the calculation method mentioned above, the gas yields for all types of shales steadily decrease with increasing oil (EOM in this study) expulsion efficiency (Fig. 7b). Furthermore, the higher the EOM potential is, the more significant the oil expulsion efficiency effect on late gas yield is. For example, when the oil expulsion efficiency increases from 40 to 60%, the late gas yield of Sample A (type I kerogen, high EOM generation potential) is reduced from 374 to 332 mL /g TOC_{Shale}, with a decrease of 42 mL/g TOC_{Shale}; whereas it is reduced from 234 to 205 mL/g TOC_{Shale}, a decrease of only 29 mL/g TOC_{Shale} for Sample E (type IIB kerogen, low EOM generation potential). This indicates that the gas generation potential for oil-prone shales is strongly affected by oil expulsion efficiency. When the oil expulsion efficiencies for different types of shales reach their upper limit values, their cumulative gas yields at 3.5% EqVRo are quite similar and range between 160 and 175 mL/g TOC_{Shale} (168 mL/g TOC_{Shale} on average, Fig. 7b).
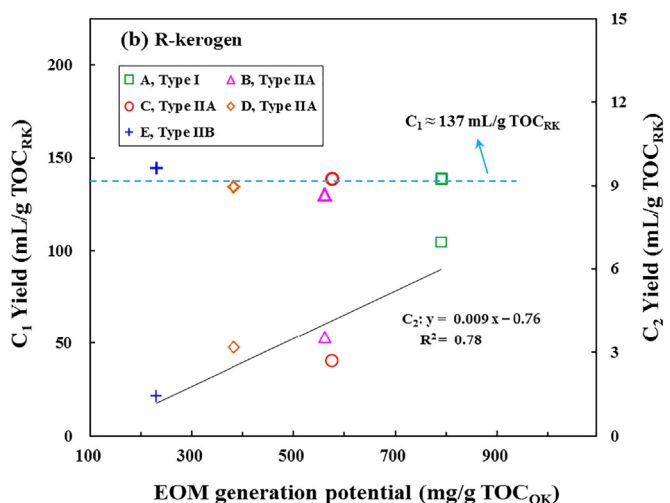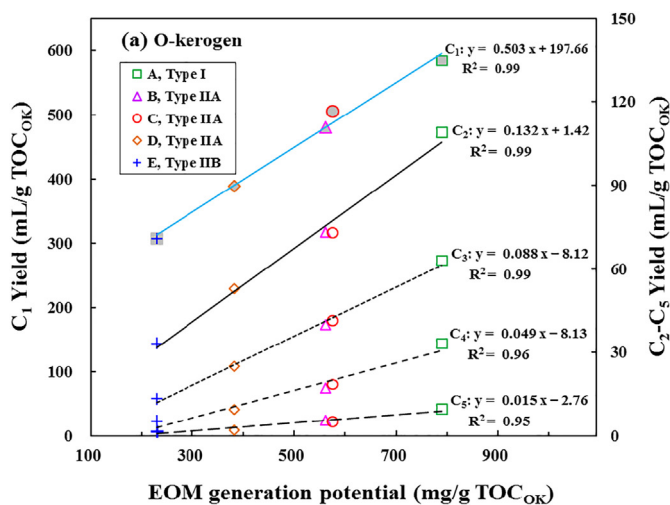
Fig. 6. Relationship between the maximum yields of individual hydrocarbon gas generated from the two series of kerogens and the EOM generation potentials of original kerogens.

3.5.2. Model of gas generation

Many studies have shown that it is quite difficult to quantitatively evaluate the oil expulsion efficiency of a shale source rock bed because it may be affected by many geological factors (Leythaeuser et al., 1988; Sandvik et al., 1992; Lafargue et al., 1994; Pepper and Corvi, 1995; Ritter, 2003; Eseme et al., 2007; Uguna et al., 2012; Ziegs et al., 2017), and this makes it difficult to assess and predict the gas amount using the relationship between gas potential and oil expulsion efficiency. However, the amount of retained EOM and the total organic carbon (TOC) content for shales are relatively easier to determine since more and more data of retained oil content are being available due to the exploration of shale oils (Jarvie, 2012b; Han et al., 2015; Cao et al., 2017). Therefore, establishing a relationship between gas yields and the amount of retained EOM can be more effectively used to predict the gas generated in geological conditions.

With the conversion of oil expulsion efficiency to the amount of retained EOM that is measured in unit of mg/g TOC_{Shale}, Fig. 7b can be transformed to form a more concise model (Fig. 8a). There is a fairly good linear and positive correlation between the gas yields and the amount of retained EOM for various types of shales (Fig. 8a), and a logarithmic relationship between the contribution ratio of EOM-cracking gas and the retained EOM content (Fig. 8b). It is also evident that the gas yields and the relative proportion of gases derived from the
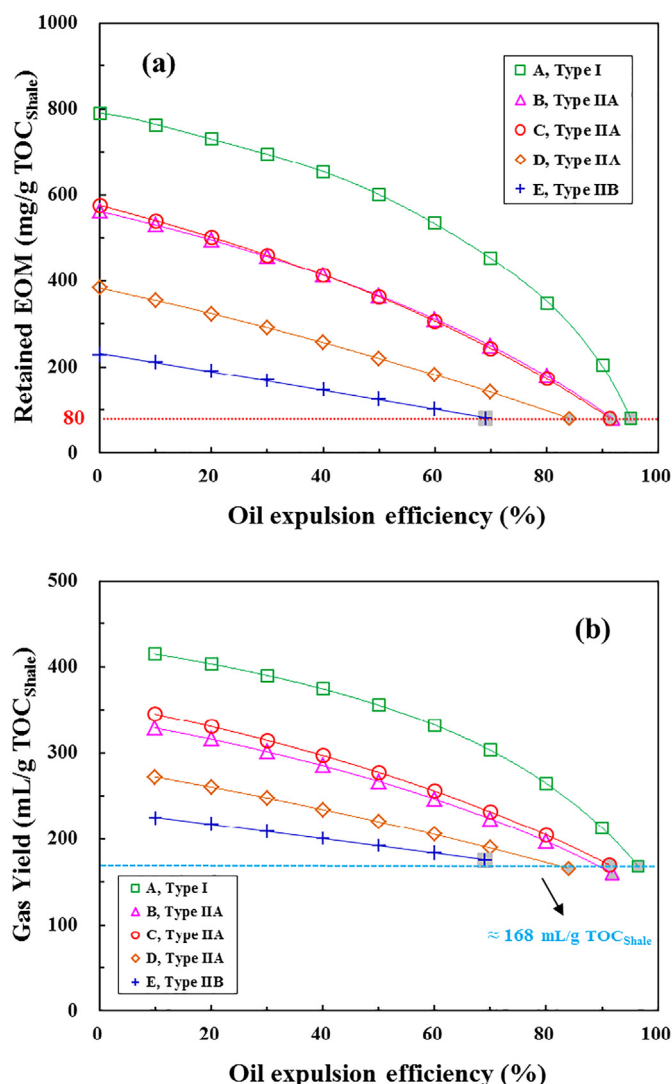
Fig. 7. Changes in the retained EOM content and the late gas generation potential (at EqVRo = 3.5%) of different types of shales with various oil expulsion efficiencies. The minimum retained EOM content is assumed to be 80 mg/g TOC_{Shale} (Jarvie, 2012b; Li et al., 2016; Cao et al., 2017) and the filled symbols represents the upper limit of their oil expulsion efficiency.
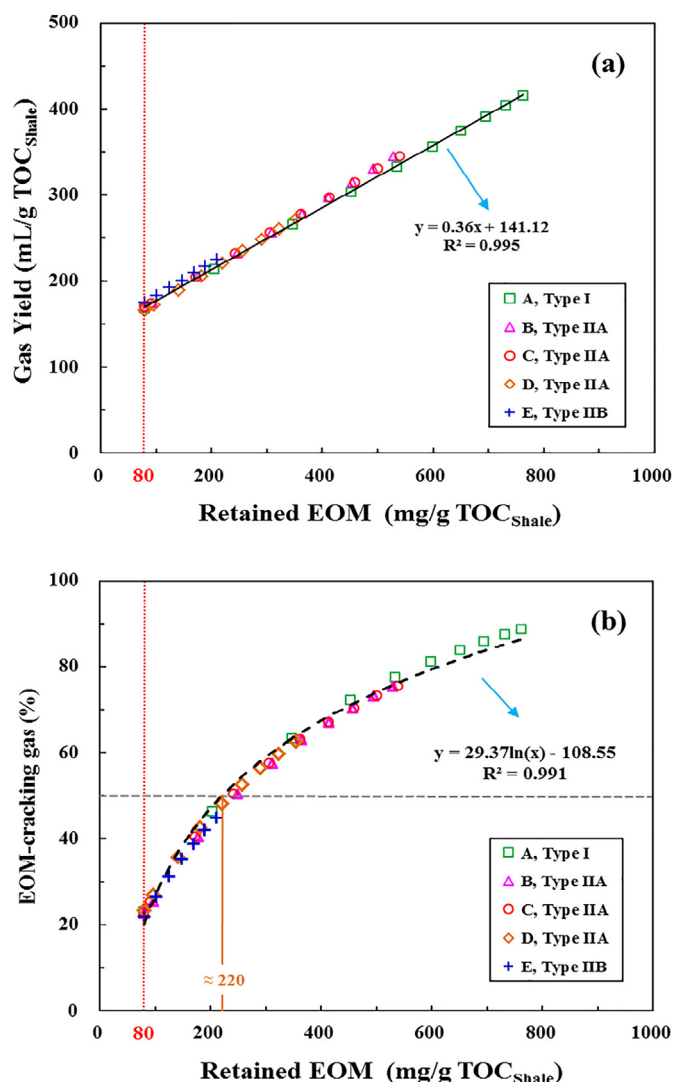

Fig. 8. A concise models illustrating the late gas generation potential of shales (a) and the relative percentages of EOM-cracking gas (b) at 3.5% EqVRo. The intercept of the regressed lines in (a) indicate the gas yield of R-kerogens is 141.12 mL/g TOC_{Shale}, whereas the slope is related to the gas yields of retained EOM. For different types of shales, their gas generation potentials are similar when they contain the same amount of retained EOMs. When the amount of retained EOM is greater than 220 mg/g TOC_{Shale}, the EOM-cracking gas would account for over 50% of the total gas generated from shales at 3.5% EqVRo.

retained EOM are quite similar for different types of shales when they have the same content of retained EOM (Fig. 8). A further examination of the linear equations in Fig. 8a reveals that the intercept represents the value of gas yield for the R-kerogens, and the slope is related to the gas yield of retained EOM. In addition, the contribution of EOM-cracking gas to the total gas will exceed more than 50% when the amount of retained EOM is greater than 220 mg/g TOC_{Shale} (Fig. 8b). For the sample A (type I O-kerogen), the retained EOM content will be more than 220 mg/g TOC_{Shale} as long as the oil expulsion efficiency is less than 89% (Fig. 8a), whereas it needs lower than 50% for Sample D (type IIA O-kerogen), and even less than 5% for Sample E (type IIB O-kerogen). Therefore, natural gas generated from oil-prone shale source rocks may be dominated by EOM-cracking gas whereas that from type IIB kerogen or gas-prone shales will be more kerogen-gas under general geological conditions. In addition, the dominance of kerogen-gas for type IIB kerogens may be further strengthened when the neo-formed organic matter is taken into account that is derived from the interaction between retained oils/EOMs and residual kerogen (Erdmann and Horsfield, 2006; Mahlstedt and Horsfield, 2012). The present exploration practice of shale oil shows that the amount of retained EOM in a shale bed may vary in the range of 100–400 mg/g TOC_{Shale} (Jarvie,

2012b; Han et al., 2015; Cao et al., 2017), and therefore, the late gas generation potential of shale source rock would approximately between 180 and 300 mL/g TOC_{Shale} (Fig. 9) under general geologic conditions when the shale oil plays are matured to 3.5% EqVRo and evolve to be shale gas plays.

3.5.3. Implications for the lower limit of gas generation potential of shales

The aforementioned results show that there are many factors affecting the late gas generation potential of shales (Figs. 7–9). For a real geological system, a large amount of gases would be generated from mature kerogen and retained EOM in shale source rock over gas-window maturity. When these hydrocarbon gases are expelled out of the shales, they may form conventional gas reservoirs; otherwise they may occur as shale gas. Although the precise reconstruction of oil expulsion process for presently overmature shale bed is difficult, it is possible to estimate its minimal gas generation potential when the shale has the minimum amount of retained EOM (i.e., 80 mg/g TOC_{Shale}). According to the experimental results and the calculation methods in
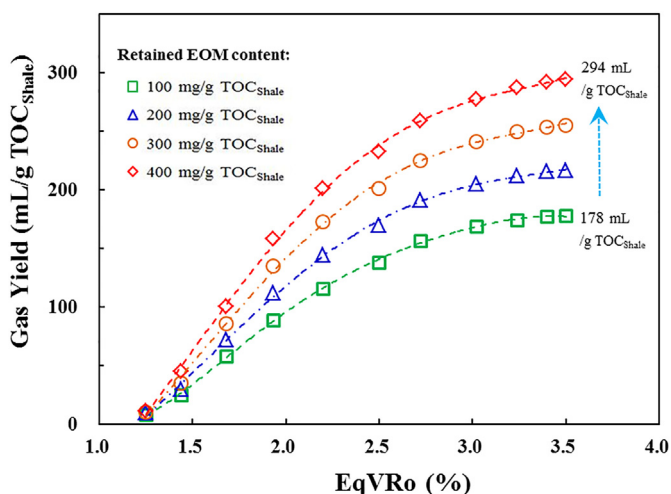
Fig. 9. Changes in late gas generation potential of shales containing type IIA kerogen (Sample C) with different amounts of retained EOMs during thermal maturation process.
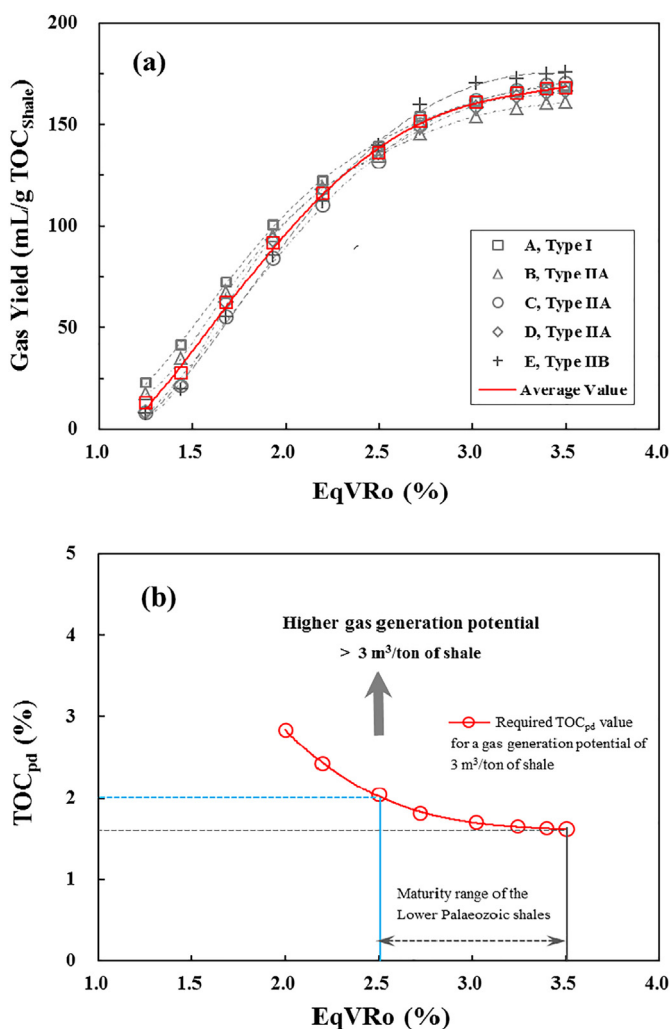

Fig. 10. Changes in the minimum gas yields of types I and II shales (a), and the conservative TOC_{pd} (present day TOC) required for a gas content of $3\,m^3$/ton of shale with increasing thermal maturity (b). The gas yields would be enhanced and hence the required TOC_{pd} value can be lowered when the amounts of retained EOM increase.

Section 3.5.1, the minimum gas yields are calculated for different shales. Similar to the gas yields of R-kerogens, the minimum gas yields for different types of shales are quite similar (Fig. 10a). For example, the minimum gas yields for shales containing types I and II kerogens vary from 132 to 139 mL/g TOC_{Shale} at 2.5% EqVRo, and between 160 and 175 mL/g TOC_{Shale} at 3.5% EqVRo.

As illustrated in Fig. 10a, the average values of the minimal gas yields which are calculated based on the minimum amount of retained EOM (i.e., 80 mg/g TOC_{Shale}) for different types of shales are approximately 100, 135, 160, and 168 mL/g TOC_{Shale} at EqVRo = 2.0%, 2.5%, 3.0%, and 3.5%, respectively. The gas yields would be enhanced by an increase in EOM retention (i.e., smaller oil expulsion efficiency). Based on the above mentioned minimum gas yields, a conservative total organic carbon content can be calculated for a specific gas yield at given thermal maturity levels. Note that the above-mentioned TOC_{Shale} is the total organic carbon content of a shale sample that has been matured to 1.22% EqVRo and contains both residual kerogen and retained EOMs, and the TOC_{Shale} could be further decreased by approximately 0–10% during the process of gas generation at maturity levels greater than 1.22% EqVRo (Jarvie et al., 2007; Vandenbroucke and Largeau, 2007). Therefore, the conservative total organic carbon values of present-day overmature shale bed (TOC_{pd}) can be further calculated according to the TOC_{Shale} values (Fig. 10b). Under the least favorable gas generation conditions (i.e., minimum retained EOM), for example, the TOC_{pd} of the shale source rock must be greater than 1.6% to have a gas yield of $3\,m^3$/ ton shale at 3.5% EqVRo, a minimum gas content for a commercial shale gas play (Halliburton Company, see details in Zou et al., 2010). In fact, the TOC_{pd} value can be further lowered if the amount of retained EOMs is higher than 80 mg/g TOC_{Shale}. Nevertheless, the gas generation potential in any cases would be greater than $3\,m^3$/ton shale at EqVRo 3.5%, as long as the TOC_{pd} of the overmature shale is greater than 1.6%.

Although the preservation conditions are equally important for shale gas reservoirs, sufficient gas generation potential is always a prerequisite and material basis for gas accumulation. Therefore the adoption of such a conservative TOC_{pd} value as a screening parameter can substantially reduce the risk of insufficient gas generation for less explored shales in complex areas such as the Lower Palaeozoic shales in South China (Zou et al., 2010, 2015; Xiao et al., 2013, 2015; Dai et al., 2014; Tian et al., 2013, 2015). For example, the thermal maturity levels of the Lower Palaeozoic shales are predominantly in the range of 2.5–3.5% EqVRo (Xiao et al., 2013), and the corresponding minimum gas yields are between 135 and 168 mL/g TOC_{Shale} (Fig. 10a). To reach a gas content of $3\,m^3$/ton shale, the conservative TOC_{pd} value of shales has to be approximately 2.0% at 2.5% EqVRo and 1.6% at 3.5% EqVRo (Fig. 10b). Therefore, a conservative TOC_{pd} value of 2.0% can be proposed as a screening parameter for the overmature shale gas exploration in the Lower Palaeozoic shales of South China. This value is quite consistent with the actual values of mostly shale gas producing areas (Curtis, 2002; Hill et al., 2007; Jarvie et al., 2007; Jarvie, 2012a; Dai et al., 2014). Therefore, the rationality of using shale TOC value for evaluation shale gas potential is confirmed by the experimental result in this study. Note that this cutoff value of TOC_{pd} is only used to eliminate the risk of insufficient gas generation for shale gas exploration. When the loss of shale gas during tectonic uplift is taken into account, the required TOC_{pd} value should be somehow enhanced but needs to be specifically assessed in terms of gas diffusion capacity that is closely related to the permeability of shales and their tectonic settings.

4. Conclusions

Different types of shale kerogen samples were pyrolyzed in sealed gold tubes under constant pressure and non-isothermal heating conditions to investigate their gas yields when their generated extractable organic matter are completely retained in or expelled out of the shales. Based on the experimental results, an evaluation model for

reconstructing the gas potential of overmature shale source rocks was tentatively proposed. The main conclusions are summarized as below.

(1) The extractable organic matter and gas generation potential of different types of original shale kerogens in a closed system vary widely in the range of 229–790 mg/g TOC_{OK} and 308–594 mL/g TOC_{OK}, respectively. The maximum gas yields of different types of residual shale kerogens after EqVRo > 1.22% are quite similar and vary between 131 and 145 mL/g TOC_{RK} at 3.5% EqVRo. However, their gas potential may be even larger in natural maturity sequences and become more distinct when the neoformed organic matter is taken into account (Mahlstedt and Horsfield, 2012).
(2) The late gas generation potential (EqVRo > 1.22%) of a shale is mainly controlled by its oil expulsion efficiency (i.e., the amount of retained EOM in this study). For different types of shales, the gas generation potentials are similar when they contain the same amount of retained EOM. Under most geologic conditions, the late gas generation potentials of shale source rock vary approximately in the range of 180–300 mL/g TOC_{Shale}.
(3) The minimum gas yields for shale source rocks containing types I-II kerogens are found to be similar, approximately 135 mL/g TOC_{Shale} at 2.5% EqVRo and 168 mL/g TOC_{Shale} at 3.5% EqVRo. Based on a gas content of 3 m^3/ton shale, a conservative present-day TOC (TOC_{pd}) of 2.0% was proposed as a screening parameter for over-mature shale gas exploration in the Lower Palaeozoic shales of South China.

Acknowledgments

Nomenclature

EOM	solvent extractable organic matter
M_O	EOM generation potential of O-kerogen samples
C_O	percentage of element carbon of generated EOM
Ro	measured vitrinite reflectance
EasyRo	calculated vitrinite reflectance with the model of Sweeney and Burnham (1990)
EqVRo	equivalent vitrinite reflectance calculated with the model of Tang et al. (1996)
TOC	total organic carbon content
TOC_{OK}	total organic carbon content of the original kerogen sample used in this study that is capable of generating both oils or EOMs and late gases
TOC_{RK}	total organic carbon content of the residual kerogen sample used in this study that was matured to 1.22% EqVRo and is only capable of generating late gases
TOC_{Shale}	total organic carbon content of both residual kerogen and retained oils or EOMs in the matured shale or kerogen sample that has been depleted of oil or EOM generation potential (e.g., EqVRo = 1.22% in this study)
TOC_{pd}	total organic carbon content of a shale sample that contains both residual kerogen and retained oils or EOMs and has EqVRo greater than 1.22%

References

Allen, M.B., Macdonald, D.I.M., Xun, Z., Vincent, S.J., Brouet-Menzies, C., 1997. Early Cenozoic two-phase extension and late Cenozoic thermal subsidence and inversion of the Bohai Basin, northern China. Mar. Pet. Geol. 14, 951–972.

Behar, F., Vandenbrouke, M., Teermann, S.C., Hatcher, P.G., Leblond, C., Lerat, O., 1995. Experimental simulation of gas generation from coals and a marine kerogen. Chem. Geol. 126, 247–260.

Behar, F., Vandenbroucke, M., Tang, Y.C., Marquis, F., Espitalié, J., 1997. Thermal cracking of kerogen in open and closed systems: determination of kinetic parameters and stoichiometric coefficients for oil and gas generation. Org. Geochem. 26, 321–339.

Behar, F., Ungerer, P., Kressmann, S., Rudkiewicz, J.L., 2006. Thermal evolution of crude oils in sedimentary basins: experimental simulation in a confined system and kinetic modeling evolution. Oil Gas Sci. Technol. 46 (2), 151–181.

Berner, U., Faber, E., 1996. Empirical carbon isotope/maturity relationships for gases from algal kerogens and terrigenous organic matter, based on dry, open-system pyrolysis. Org. Geochem. 24, 947–955.

Braun, R.L., Burnham, A.K., 1990. Mathematical model of oil generation, degradation, and expulsion. Energy Fuel 4 (2), 132–146.

Cao, H.R., Zou, Y.R., Lei, Y., Xi, D.P., Wan, X.Q., Peng, P.A., 2017. Shale oil assessment for the Songliao Basin, northeastern China, using oil generation-sorption method. Energy Fuel 31, 4826–4842.

Cooles, G.P., Mackenzie, A.S., Quigley, T.M., 1986. Calculation of petroleum masses generated and expelled from source rocks. Org. Geochem. 10, 235–245.

Curtis, J.B., 2002. Fractured shale-gas systems. AAPG Bull. 86 (11), 1921–1938.

Curtis, M.E., Cardott, B.J., Sondergeld, C.H., Rai, C.S., 2012. Development of organic porosity in the woodford shale with increasing thermal maturity. Int. J. Coal Geol. 103 (23), 26–31.

Dai, J.X., Song, Y., Zhang, H.F., 1997. Main factors controlling the foundation of medium-giant gas fields in China. China Ser. B Earth Sci. 40 (1), 1–10.

Dai, J.X., Zou, C.N., Liao, S.M., Dong, D.Z., Ni, Y.Y., Huang, J.L., Wu, W., Gong, D.Y., Huang, S.P., Hu, G.Y., 2014. Geochemistry of the extremely high thermal maturity Longmaxi shale gas, southern Sichuan Basin. Org. Geochem. 74, 3–12.

Dieckmann, V., Schenk, H.J., Horsfield, B., Welte, D.H., 1998. Kinetics of petroleum generation and cracking by programmed-temperature closed-system pyrolysis of Toarcian shales. Fuel 77 (1–2), 23–31.

Dieckmann, V., Ondrak, R., Cramer, B., Horsfield, B., 2006. Deep basin gas: new insights from kinetic modelling and isotopic fractionation in deep-formed gas precursors. Mar. Pet. Geol. 23, 183–199.

Erdmann, M., Horsfield, B., 2006. Enhanced late gas generation potential of petroleum source rocks via recombination reactions: evidence from the Norwegian North Sea. Geochim. Cosmochim. Acta 70, 3943–3956.

Eseme, E., Littke, R., Krooss, B.M., Schwarzbauer, J., 2007. Experimental investigation of the compositional variation of petroleum during primary migration. Org. Geochem. 38, 1373–1397.

Eseme, E., Krooss, B.M., Littke, R., 2012. Evolution of petrophysical properties of oil shales during high-temperature compaction tests: implications for petroleum expulsion. Mar. Pet. Geol. 31 (1), 110–124.

Feng, Z.Q., Jia, C.Z., Xie, X.N., Zhang, S., Feng, Z.H., Cross, T.A., 2010. Tectonostratigraphic units and stratigraphic sequences of the nonmarine Songliao Basin, northeast China. Basin Res. 22 (1), 79–95.

Feng, Y., Jiang, S., Hu, S., Li, S., Lin, C., Xie, X., 2016. Sequence stratigraphy and importance of syndepositional structural slope-break for architecture of Paleogene syn-rift lacustrine strata, Bohai Bay Basin, E. China. Mar. Pet. Geol. 69, 183–204.

Gai, H.F., Xiao, X.M., Cheng, P., Tian, H., Fu, J.M., 2015. Gas generation of shale organic matter with different contents of residual oil based on a pyrolysis experiment. Org. Geochem. 78, 69–78.

Galimov, E.M., 1988. Sources and mechanisms of formation of gaseous hydrocarbons in sedimentary rocks. Chem. Geol. 71 (1), 77–95.

Guo, L.G., Xiao, X.M., Tian, H., Song, Z.G., 2009. Distinguishing gases derived from oil cracking and kerogen maturation: insights from laboratory pyrolysis experiments. Org. Geochem. 40, 1074–1084.

Guo, X., Liu, K., He, S., Song, G., Wang, Y., Hao, X., Wang, B., 2012. Petroleum generation and charge history of the northern Dongying Depression, Bohai Bay Basin, China: insight from integrated fluid inclusion analysis and basin modelling. Mar. Pet. Geol. 32, 21–35.

Han, Y.J., Mahlstedt, N., Horsfield, B., 2015. The Barnett Shale: compositional fractionation associated with intraformational petroleum migration, retention, and expulsion. AAPG Bull. 99 (12), 2173–2202.

Hao, F., Guo, T.L., Zhu, Y.M., Cai, X.Y., Zou, H.Y., Li, P.P., 2008. Evidence for multiple stages of oil cracking and thermochemical sulfate reduction in the Pugang gas field, Sichuan Basin, China. AAPG Bull. 92 (5), 611–637.

Hao, F., Zhou, X., Zhu, Y., Yang, Y., 2011. Lacustrine source rock deposition in response to co-evolution of environments and organisms controlled by tectonic subsidence and climate, Bohai Bay Basin, China. Org. Geochem. 42, 323–339.

Hill, R.J., Tang, Y.C., Kaplan, I.R., 2003. Insights into oil cracking based on laboratory experiments. Org. Geochem. 34, 1651–1672.

Hill, R.J., Jarvie, D.M., Zumberge, J., Henry, M., Pollastro, M., 2007. Oil and gas geochemistry and petroleum systems of the Fort Worth Basin. AAPG Bull. 91, 445–473.

Hsiao, L.Y., Graham, S.A., Tilander, N., 2004. Seismic reflection imaging of a major strikeslip fault zone in a rift system: Paleogene structure and evolution of the Tan-Lu fault system, Liaodong Bay, Bohai, offshore China. AAPG Bull. 88, 71–97.

Hu, S., O'Sullivan, P.B., Raza, A., Kohn, B.P., 2001. Thermal history and tectonic subsidence of the Bohai Basin, northern China: a Cenozoic rifted and local pull-apart basin. Phys. Earth Planet. Inter. 126, 221–235.

Jarvie, D.M., 2012a. Shale resource systems for oil and gas: Part 1—Shale-gas resource systems. In: Breyer, J.A. (Ed.), Shale Reservoirs–Giant Resources for the 21st Century: AAPG Memoir. vol. 97. pp. 69–87.

Jarvie, D.M., 2012b. Shale resource systems for oil and gas: part 2—shale-oil resource systems. In: Breyer, J.A. (Ed.), Shale Reservoirs–Giant Resources for the 21st Century:

AAPG Memoir. vol. 97. pp. 89–119.

Jarvie, D.M., Hill, R.J., Ruble, T.E., Pollastro, R.M., 2007. Unconventional shale-gas systems: the Mississippian Barnett Shale of north-central Texas as one model for thermogenic shale-gas assessment. AAPG Bull. 91 (4), 475–499.

Jia, J., Bechtel, A., Liu, Z., Strobl, S.A.I., Sun, P., Sachsenhofer, R.F., 2013. Oil shale formation in the Upper Cretaceous Nenjiang Formation of the Songliao Basin (NE China): implications from organic and inorganic geochemical analyses. Int. J. Coal Geol. 113, 11–26.

Jia, W.L., Wang, Q.L., Liu, J.Z., Peng, P.A., Li, B.H., Lu, J.L., 2014. The effect of oil expulsion or retention on further thermal degradation of kerogen at the high maturity stage: a pyrolysis study of type II kerogen from Pingliang shale, China. Org. Geochem. 71, 17–29.

Lafargue, W., Espitalié, J., Broks, T.M., Nyland, B., 1994. Experimental simulation of primary migration. Org. Geochem. 22, 575–586.

Lafargue, F., Marquis, F., Pillot, D., 2006. Rock-Eval 6 applications in hydrocarbon exploration, production, and soil contamination studies. Oil Gas Sci. Technol. 53 (4), 421–437.

Leythaeuser, D., Radke, M., Schaefer, R.G., 1984. Efficiency of petroleum expulsion from shale source rocks. Nature 311, 745–748.

Leythaeuser, D., Schaefer, R.G., Radke, M., 1988. Geochemical effects of primary migration of petroleum in Kimmeridge source rocks from Brae field area, North Sea. I: gross composition of C_{15}^+-soluble organic matter and molecular composition of C_{15}^+-saturated hydrocarbons. Geochim. Cosmochim. Acta 52, 701–713.

Li, Z., Zou, Y.R., Xu, X.Y., Sun, J.N., Li, M., Peng, P.A., 2016. Adsorption of mudstone source rock for shale oil – experiments, model and a case study. Org. Geochem. 92, 55–62.

Lorant, F., Behar, F., 2002. Late generation of methane from mature kerogens. Energy Fuel 16 (2), 412–427.

Ma, Y.S., Guo, X.S., Guo, T.L., Huang, R., Cai, X.Y., Li, G.X., 2007. The Puguang gas field: new giant discovery in the mature Sichuan Basin, southwest China. AAPG Bull. 91, 627–643.

Ma, Y.S., Zhang, S.C., Guo, T.L., Zhu, G.Y., Cai, X.Y., Li, M.W., 2008. Petroleum geology of the Puguang sour gas field in the Sichuan Basin, SW China. Mar. Pet. Geol. 25, 357–370.

Ma, Y.Q., Fan, M.J., Lu, Y.C., Liu, H.M., Hao, Y.Q., Xie, Z.H., Peng, L., Du, X.B., Hu, H.Y., 2017. Middle Eocene paleohydrology of the dongying depression in eastern china from sedimentological and geochemical signatures of lacustrine mudstone. Palaeogeogr. Palaeoclimatol. Palaeoecol. 479, 16–33.

Mahlstedt, N., Horsfield, B., 2012. Metagenetic methane generation in gas shales I. Screening protocols using immature samples. Mar. Pet. Geol. 31, 27–42.

Mahlstedt, N., Horsfield, B., Dieckmann, V., 2008. Second order reactions as a prelude to gas generation at high maturity. Org. Geochem. 39, 1125–1129.

Modica, C.J., Lapierre, S.G., 2012. Estimation of kerogen porosity in source rocks as a function of thermal transformation: example from the Mowry Shale in the Powder River Basin of Wyoming. AAPG Bull. 96 (1), 87–108.

Mukhopadhyay, P.K., Wade, J.A., Kruge, M.A., 1995. Organic facies and maturation of Jurassic/Cretaceous rocks, and possible oil-source rock correlation based on pyrolysis of asphaltenes, Scotion Basin, Canada. Org. Geochem. 22, 85–104.

Ozkaya, I., Akbar, A., 1991. An interative procedure to determine depth and time of primary oil migration and expulsion efficiency of source rocks. J. Pet. Sci. Eng. 5, 371–378.

Pan, C.C., Jiang, L.L., Liu, J.Z., Zhang, S.C., Zhu, G.Y., 2010. The effects of calcite and montmorillonite on oil cracking in confined pyrolysis experiments. Org. Geochem. 41 (7), 611–626.

Pan, C.C., Jiang, L.L., Liu, J.Z., Zhang, S.C., Zhu, G.Y., 2012. The effects of pyrobitumen on oil cracking in confined pyrolysis experiments. Org. Geochem. 45, 29–47.

Pepper, A.S., Corvi, P.J., 1995. Simple kinetic models of petroleum formation. Part III: modelling an open system. Mar. Pet. Geol. 12, 417–452.

Peters, K.E., Cassa, M.R., 1994. Applied source rock geochemistry. In: Magoon, L.B., Dow, W.G. (Eds.), The Petroleum System-from Source to Trap. AAPG Bull 60. pp. 93–120.

Ritter, U., 2003. Solubility of petroleum compounds in kerogen: implications for petroleum expulsion. Org. Geochem. 34, 319–326.

Sandvik, E.I., Young, W.A., Curry, D.J., 1992. Expulsion from hydrocarbon sources: the role of organic absorption. Org. Geochem. 19, 77–87.

Stainforth, J.G., Reinders, J.E., 1990. Primary migration of hydrocarbons by diffusion through organic matter networks, and its effect on oil and gas generation. Org. Geochem. 16, 61–74.

Sweeney, J.J., Burnham, A.K., 1990. Evaluation of a simple model of vitrinite reflectance based on chemical kinetics. AAPG Bull. 74, 1559–1570.

Tang, Y.C., Jenden, P.D., Nigrini, A., Teerman, S.C., 1996. Modeling early methane generation in coal. Energy Fuel. 10, 659–671.

Tian, H., Wang, Z.M., Xiao, Z.Y., Li, X.Q., Xiao, X.M., 2006. Oil cracking to gases: kinetic modeling and geological significance. Chin. Sci. Bull. 51, 2763–2770.

Tian, H., Xiao, X.M., Yang, L.G., Xiao, Z.Y., Guo, L.G., Shen, J.G., Lu, Y.H., 2009. Pyrolysis of oil at high temperatures: gas potentials, chemical and carbon isotopic signatures. Chin. Sci. Bull. 54 (7), 1217–1224.

Tian, H., Xiao, X.M., Wilkins, R.W.T., Tang, Y.C., 2012. An experimental comparison of gas generation from three oil fractions: implications for the chemical and stable carbon isotopic signatures of oil cracking gas. Org. Geochem. 46, 96–112.

Tian, H., Pan, L., Xiao, X.M., Wilkins, R.W.T., Meng, Z.P., Huang, B.J., 2013. A preliminary study on the pore characterization of Lower Silurian black shales in the Chuandong Thrust Fold Belt, Southwestern China using low pressure N_2 adsorption and FE-SEM methods. Mar. Pet. Geol. 48, 8–19.

Tian, H., Pan, L., Zhang, T.W., Xiao, X.M., Meng, Z.P., Huang, B.J., 2015. Pore characterization of organic-rich Lower Cambrian shales in Qiannan Depression of Guizhou Province, southwestern China. Mar. Pet. Geol. 62, 28–43.

Tissot, B.P., Welte, D.H., 1984. Petroleum Formation and Occurrence: A New Approach to Oil and Gas Exploration. Springer, Berlin, Heidelberg, pp. 699.

Uguna, C.N., Carr, A.D., Snape, C.E., Meredith, W., Díaz, M.C., 2012. A laboratory pyrolysis study to investigate the effect of water pressure on hydrocarbon generation and maturation of coals in geological basins. Org. Geochem. 52, 103–113.

Ungerer, P., 1988. Kinetic modeling of oil cracking. Org. Geochem. 13 (4), 857–868.

Ungerer, P., 2003. From organic geochemistry to statistical thermodynamics: the development of simulation methods for the petroleum industry. Angew. Chem. Int. Ed. 58 (2), 271–297.

Vandenbroucke, M., Largeau, C., 2007. Kerogen origin, evolution and structure. Org. Geochem. 38 (5), 719–833.

Wei, Z.F., Zou, Y.R., Cai, Y.L., Wang, L., Luo, X.R., Peng, P.A., 2012. Kinetics of oil group-type generation and expulsion: an integrated application to Dongying Depression, Bohai Bay Basin, China. Org. Geochem. 52, 1–12.

Xiao, X.M., Zeng, Q.H., Tian, H., Wilkins, R.W.T., Tang, Y.C., 2005. Origin and accumulation model of the AK-1 natural gas pool from the Tarim Basin, China. Org. Geochem. 36, 1285–1298.

Xiao, X.M., Song, Z.G., Zhu, Y.M., Tian, H., Yin, H.W., 2013. Summary of shale gas research in North American and revelations to shale gas exploration of Lower Paleozoic strata in South China area. J. China Coal Soc. 38 (5), 721–727 (in Chinese).

Xiao, X.M., Wei, Q., Gai, H.F., Li, T.F., Wang, M.L., Pan, L., Chen, J., Tian, H., 2015. Main controlling factors and enrichment area evaluation of shale gas of the Lower Paleozoic marine strata in South China. Pet. Sci. 12, 573–586.

Xie, L.J., Sun, Y.G., Jiang, A.Z., Wang, F.Y., Chen, J.P., 2015. Experimental study on the gas generation processes of lacustrine and marine shales in North China: source implications for shale gas. Mar. Pet. Geol. 67, 204–216.

Xiong, Y.Q., Zhang, L., Chen, Y., Wang, X.T., Li, Y., Wei, M.M., Jiang, W.M., Lei, R., 2016. The origin and evolution of thermogenic gases in organic-rich marine shales. J. Pet. Sci. Eng. 143, 8–13.

Ye, H., Shedlock, K.M., Hellinger, S.J., Sclater, J.G., 1985. The North China Basin: an example of a Cenozoic rifted intraplate basin. Tectonics 4, 153–169.

Zhao, W.Z., Wang, Z.Y., Zhang, S.C., Wang, H.J., Zhao, C.Y., Hu, G.Y., 2005. Successive generation of natural gas from organic materials and its significance in future exploration. Pet. Explor. Dev. 32 (2), 1–7 (in Chinese).

Ziegs, V., Horsfield, B., Skeie, J.E., Rinna, J., 2017. Petroleum retention in the Mandal Formation, Central Graben, Norway. Mar. Pet. Geol. 83, 195–214.

Zou, C.N., Dong, D.Z., Wang, S., Li, J., Li, X., Wang, Y., Li, D., 2010. Geological characteristics and resource potential of shale gas in China. Pet. Explor. Dev. 37, 641–653 (in Chinese).

Zou, C.N., Du, J.H., Xu, C.C., Wang, Z.C., Zhang, B.M., Wei, G.Q., Wang, T.S., Yao, G.S., Deng, S.H., Liu, J.J., Zhou, H., Xu, A.N., Yang, Z., Jiang, H., Gu, Z.D., 2014. Formation, distribution, resource potential and discovery of the Sinian−Cambrian giant gas field, Sichuan Basin, SW China. Pet. Explor. Dev. 41 (3), 306–325.

Zou, C.N., Dong, D.Z., Wang, Y.M., Li, X.J., Huang, J.L., Wang, S.F., Guan, Q.Z., Zhang, C.C., Wang, H.Y., Liu, H.L., Bai, W.H., Liu, D.X., Yang, Z., Liang, P.P., Sun, S.S., Qiu, Z., 2015. Shale gas in China: characteristics, challenges and prospects (II). Pet. Explor. Dev. 43 (6), 753–767.